Article:

INTERCHAIN SPACING AND SCREENING LENGTH MODIFICATION OF PSS BACKBONE CHAINS IN ZWITTERION DOPED POLY(3,4-ETHYLENEDIOXYTHIOPHENE):POLYSTYRENE SULFONATE

Gabriel E. Pérez[a],* Ali Alkorbi[b], Ahmed Iraqi[b], Francesco Bastianini[a], Edwin Pineda[a], Stephen M. King[c], Alan D. F. Dunbar[a]

[a]*Department of Chemical and Biological Engineering, Faculty of Engineering, University of Sheffield, S1 3JD, Sheffield, UK*

e-mail:* geperez1@sheffield.ac.uk

e-mail: a.dunbar@sheffield.ac.uk

[b]*Department of Chemistry, Faculty of Engineering, University of Sheffield, S3 7HF, Sheffield, UK*

[c]*ISIS Pulsed Neutron and Muon Source, STFC, Rutherford Appleton Laboratory, OX11 0QX, Didcot, UK*

Abstract – The interchain spacing and screening length modification of deuterated PSS (d-PSS) backbone chains in zwitterion doped PEDOT:d-PSS were studied as a function of the doping concentration using small angle neutron scattering. Results suggest that the dopant, 3-(N,N-Dimethylmyristylammonio)propanesulfonate (DYMAP), forms worm-like micelle structures in the PEDOT:d-PSS dispersion that grow in size as the doping concentration increases. The interchain spacing between negatively charged d-PSS remains unaffected by DYMAP up to 15 mM doping concentration, however, from 15 mM to 25 mM doping concentration, the interchain spacing increases due to steric interactions of grown DYMAP worm-like micelles with the d-PSS chains. At 30 mM doping concentration, the interchain distance between negatively charged d-PSS chains is reduced due to the gelation of the PEDOT:d-PSS dispersion caused by the crosslinking between long DYMAP worm-like micelles and d-PSS chains. Meanwhile, the screening length of the neutralised d-PSS segments attached to the PEDOT oligomers increases as the DYMAP concentration increases form 5 mM to 30 mM due to the neutralisation of the negatively charged d-PSS segments by their coulombic interaction with the cation in DYMAP.

Keywords: PEDOT:PSS, small angle neutron scattering, zwitterion, deuteration, correlation length, charge screening, interchain spacing.

INTRODUCTION

Poly(3,4-ethylenedioxythiophene) polystyrene sulfonate (PEDOT:PSS) is one of the most widely used conducting polymers [1], with applications that range from OLED based displays [2, 3] and solar cells [4, 5], to bone regeneration [6] and nanobiointerfaces [7, 8]. This is due to its numerous advantageous characteristics such as its biocompatibilty [9, 10], good thermal and mechanical stability [11-13], excellent water solubility [1], and optical transparency in the visible spectrum when processed as a thin film [14]. However, its intrinsic conductivity is relatively low compared to most inorganic conductors. A widely used technique to improve the conductivity of PEDOT:PSS is the addition of asymmetrically charged dopants such as ionic liquids [15, 16], acids [17, 18], polar solvents [19, 20], alcohols [21, 22], polyelectrolytes, salts [23-26], and surfactants [27-29]. The increase in conductivity is normally attributed to the disruption of the coulombic interactions between PEDOT and PSS by the asymmetrically charged dopant [23-26, 28-31], which is believed to promote phase separation of PEDOT and PSS resulting in a more ordered conducting network that facilitates improved charge transport when deposited as a thin film [23, 26, 32, 33]. However, despite the extensive research done on the conductivity enhancement of PEDOT:PSS by the addition of dual-charge dopants, the precise mechanisms by which the conductivity is improved are still not completely understood and can differ depending on the type of additive used [34, 35]. The lack of precise understanding of the mechanisms of conductivity enhancement poses a major barrier to furthering PEDOT:PSS engineering in order to achieve its optimal performance in its numerous applications. To fully understand the improvement of the conductivity of doped PEDOT:PSS, it is paramount to determine the structural modifications that the dopant induces within the PEDOT:PSS morphology. Small angle X-ray scattering has been used before to provide more insight on the nanoscopic behaviour of the widely studied dimethyl sulfoxide (DMSO) [36] and ethylene glycol (EG) [37] doped PEDOT:PSS while in dispersion. Following the specific changes that PEDOT and PSS go through separately has hitherto proven to be challenging due to their similar scattering length densities (SLDs). Tracking the morphological changes of PSS and PEDOT separately after doping is crucial to fully understand the origin of conductivity enhancement. Specifically, PSS is of particular interest since it is the major component of the PEDOT:PSS polymer mixture; enabling its solubility in water by countering the hydrophobicity of PEDOT [4, 38].

Using neutrons instead of x-rays as the small angle scattering probe allows the labelling of a specific component within the studied system through deuteration. Therefore, by deuterating PSS (d-PSS) it is possible to obtain its individual scattering profile and thus track its changes in isolation from the rest of the system. Using this technique, Etampawala et al. successfully determined that the addition of DMSO to a PEDOT:d-PSS dispersion results in the re-organisation of excess d-PSS, significantly reducing the amount of d-PSS rich domains which contribute to the improved conductivity of PEDOT:d-PSS when spray coated into a thin film [35]. Murphy et al. also studied a PEDOT:d-PSS dispersion using small angle neutron scattering (SANS) to determine the effects of 1-ethyl-3-methylimidazolium tetracyanoborate (EMIM:TCB) on the d-PSS chains arrangement [39]. They found that the negatively charged d-PSS backbone segments are neutralised by the EMIM cation which appears to improve the packing of the chains due to the screening of charge repulsion. Despite the insight provided by these reports, there is still a significant gap in the understanding of how other additives affect the PEDOT:PSS structural conformation. The different dopants used to improve the conductivity of PEDOT:PSS affect it differently according to the nature of the dopants requiring separate studies to achieve a complete understanding on the mechanisms of conductivity enhancement of PEDOT:PSS. For instance, zwitterions are surfactants that have proven to improve the conductivity of PEDOT:PSS and offer the advantage that their charges are fixed within the molecule so they do not migrate out of the doped PEDOT:PSS layer to other components of the device where PEDOT:PSS is used which can happen with ionic dopants [28, 29, 40]. However, surfactants behave much differently to ionic liquids such as EMIM:TCB or polar solvents such as DMSO when dissolved in an aqueous solution which suggests that the structural modifications that they induce in PEDOT:PSS are also different. In a previous neutron reflectivity study, we used the zwitterionic surfactant 3-(N,N dimethylmyristylammonio)propanesulfonate (DYMAP) to dope PEDOT:PSS and improved its conductivity by more than one order of magnitude. Additionally, we found a strong dependence between the DYMAP doping concentration and the vertical structure of the processed thin films [41]. Here, we study DYMAP doped PEDOT:d-PSS by using SANS to track the changes that PSS goes through while in dispersion as DYMAP is gradually added, and by doing so, provide a deeper understanding on the structural modification of PEDOT:d-PSS for conductivity enhancement by zwitterionic surfactant doping.

EXPERIMENTAL

MATERIALS

DYMAP ($\geq$ 98%, by TLC, CMC: 0.1-0.4 mM at 20-25ºC, 30,200 micellar average molecular weight), iron (III) sulfate hydrate (97%), deuterium oxide (99.9 atom % isotopic purity), and ion exchange resins Amberlite IR-120 (hydrogen form, strongly acidic) and Lewatit MP-62 (free base, weakly basic) were all purchased from Sigma Aldrich. Sodium persulfate ($\geq$ 98%) was purchased from ChemCruz Biochemicals while 3,4-Ethylenedioxythiophene (97%) was purchased from Alfa Aesar. Finally, deuterated poly(styrene sulfonic acid) (d7, 33,800 Mn, 1.04 Mw/Mn) was purchased from Polymer Source and deionized water was obtained from a Purelab Flex 1 dispenser.

SYNTHESIS OF PEDOT:DEUTERATED-PSS

PEDOT:d-PSS was synthesised following the BAYTRON P synthesis method developed by Bayer AG as reported several times in literature [1, 42, 43]. The PEDOT:d-PSS dispersion was synthesised in a ~34%-D_2O ~66%-H_2O solvent which is SLD matched to the calculated PEDOT SLD of 1.80 x 10^{-6} Å^{-2}. First, 4.606 mL of D_2O and 9.884 mL of H_2O were mixed in a round bottomed flask and then 0.2 g of d-PSS, 61.7 mg of EDOT, 124.2 mg of $Na_2S_2O_8$, and 1.1 mg of $Fe(SO_4)_3$ were added to the flask. The specific EDOT and d-PSS amounts were chosen to obtain a PEDOT to d-PSS ratio of ~1:2.5. The dispersion was stirred vigorously at 30ºC in an oil bath and under a condensing column for 7 hours. Then, 20.8 mg of $Na_2S_2O_8$ were added to the dispersion and stirred for a further 14 hours. When the synthesis was complete, 1 gram of each ion exchange resin was added to the flask and the dispersion was left stirring for 2 additional hours at room temperature. The dispersion was then filtered through a 0.5 mm mesh and an additional gram of each ion exchange resin was added to the filtered dispersion which was then stirred for 2 more hours. Finally, the PEDOT:d-PSS dispersion was filtered through the mesh again and a total of 5 mL of dispersion was collected and stored at 4ºC. The total solids content of the dispersion was ~ 1.75 wt.% determined by gravimetric analysis.

CHARACTERISATION

The Small Angle Neutron Scattering (SANS) data was obtained using the LOQ small-angle diffractometer [44] at the ISIS Pulsed Neutron Source (STFC Rutherford Appleton Laboratory, Didcot, UK). A 10 mm diameter pulsed neutron beam modulated at 25 Hz with an incident wavelength range of 2.2 - 10.0 Å was directed through the samples to obtain scattering data within a q range of 0.008 - 0.254 Å. The collected data were corrected for detector response and transmission of the sample using the Mantid data reduction software [45] to obtain absolute intensity vs momentum transfer 1D scattering plots. Scattering intensity data that had poor accuracy (evidenced by the wide error bars of each data point) was discarded. The reduced data was fitted with the Broad Peak model [46] using the SasView software [47]. The dispersions for the experiment were prepared by pouring 1 mL of PEDOT:d-PSS in a vial and then adding DYMAP powder in different amounts to obtain the desired concentration in millimolar units. The dispersions were stirred for 5 minutes and then loaded into cells (Hellma Macro-cuvette 404.000-QX 1mm thickness 404-2-46, Lab Unlimited) for neutron scattering measurements. The scattering length densities of PEDOT (1.80×10^{-6} Å^{-2}), d-PSS (4.18×10^{-6} Å^{-2}), DYMAP (4.67×10^{-8} Å^{-2}), H_2O (-5.61×10^{-7} Å^{-2}), and D_2O (6.39×10^{-6} Å^{-2}) were calculated using the NIST Center for Neutron Research online database [48]

RESULTS AND DISCUSSION

PEDOT and PSS have similar neutron SLDs of 1.80×10^{-6} Å^{-2} and 1.58×10^{-6} Å^{-2} respectively which makes it difficult to distinguish their scattering spectra from each other. Thus, if the solvent's SLD is contrast matched to PEDOT, the scattering signal from PSS would be lost in the background. However, d-PSS has an SLD of 4.18×10^{-6} Å^{-2} providing the necessary contrast with PEDOT to obtain a scattering signal from d-PSS when the solvent is contrast matched to PEDOT. Therefore, in order to study the change in structural conformations due to electrostatic interactions that PSS goes through after DYMAP doping, a PEDOT:d-PSS dispersion in a $D_2O\backslash H_2O$ solvent which SLD was matched to that of PEDOT was synthesised.

To study the effect that DYMAP has on d-PSS in a PEDOT:d-PSS dispersion, the small angle neutron scattering spectra of seven different DYMAP doped PEDOT:d-PSS dispersions were analysed . The seven different samples were pristine PEDOT:d-PSS, and 5 mM, 10 mM, 15 mM, 20 mM, 25 mM and 30 mM DYMAP doped PEDOT:d-PSS. Figure 1 shows the 1D SANS plot of all the samples where it can be immediately observed that the scattering intensity decreases as the DYMAP doping concentration increases. Given that the SLD of DYMAP is 4.67 x 10^{-8} Å^{-2}, the decreased intensity of the doped dispersions can be attributed to the decreased scattering contrast caused by DYMAP which, by interacting with d-PSS, reduces its SLD corroborating that the two interact at a molecular level. It is worth noting that the SLD of DYMAP is closer to the SLD of the subtracted background (solvent matched to PEDOT) than to the SLD of d-PSS and hence, most of the scattering from DYMAP gets subtracted with the background during the data reduction process.

In order to analyse the 1D scattering plots further, an empirical Broad Peak Model was fitted to the data. The model has been used before to fit neutral and charged polymer systems that exhibit electrostatic interactions, including PEDOT:PSS [39, 49]. The model is described as

$$I_{(q)} = \frac{A}{q^n} + \frac{C}{1+(|q-q_0|\xi)^m} + B \qquad (1)$$

where A/q^n is the low-q clustering term and $C/[1+(|q-q_0|\xi)^m+B]$ is the high-q solvation term. More specifically, A is the Porod law scale factor, n the low-q scaling exponent, C the Lorentzian scale factor, m the high-q exponent, ξ the screening length, q_0 is the peak position, and B the q-independent background. Table 1 shows the resulting fitting parameters for each sample. The analysis focused on two particular parameters from the model, the peak position (q_0), and the screening length (ξ). Both parameters are in the high-q solvation term of the model function that describes the interactions between the scatterer and its surrounding environment at the nano scale. First, the peak position is analysed which has a finite value for charged systems and a negligible value for neutral systems [49]. Specifically, in polyelectrolyte systems this peak is characteristic, and is caused by the interchain [50-53] spacing between the charged segments that exist along the polymer chain [54]. This was corroborated for PEDOT:PSS by Murphy et al. who, by conducting a serial dilution SANS

study of PEDOT:PSS, confirmed that the q_0 value is representative of the interchain distance between negatively charged rod-like PSS segments that are located along the PEDOT:PSS chain [39]. Therefore, for this experiment it can be safely assumed that q_0 corresponds to an average interchain distance of $2\pi/q_0$ Å^{-1} between the negatively charged d-PSS segments along the chain backbones that are not attached to the PEDOT oligomers. As shown in table 1, the pristine d-PSS sample had a q_0 of 0.0310 Å^{-1} which corresponds to an average interchain distance between charged d-PSS segments of ≈202.7 Å^{-1}. This value is similar to that reported by Murphy et al. of ≈196.4 Å^{-1} [39].

As the DYMAP doping concentration increased, a negligible change in q_0 is initially observed. The q_0 of the 5 mM, 10 mM, and 15 mM doped samples were 0.0308 Å^{-1}, 0.0307 Å^{-1}, and 0.0306 Å^{-1} respectively. Figure 2 illustrates this change where it can be clearly seen that the peak position does not significantly change when DYMAP is added up to a 15 mM concentration indicating that the average interchain distance between the charged d-PSS segments is barely perturbed by the addition of DYMAP up to this doping concentration. However, at 20 mM and 25 mM doping concentration q_0 decreases more abruptly to 0.0296 Å^{-1} and 0.0285 Å^{-1} respectively resulting in the interchain distance between d-PSS charged segments being increased by ~7 Å with each of these increased concentration steps. Interestingly, at 30 mM doping concentration the q_0 shifts back to 0.0308 Å^{-1} which means that the average interchain distance between d-PSS charged segments decreases to 203.8 Å^{-1} reverting back to the approximate same value of pristine PEDOT:d-PSS.

To understand the interchain distance change between the charged d-PSS segments induced by DYMAP, the behaviour of DYMAP alone (no PEDOT:d-PSS present in the sample) in the same aqueous solvent that the PEDOT:d-PSS is dispersed in was separately studied. The 1D scattering plot of two 30 mM DYMAP aqueous solutions was obtained, one was in D_2O/H_2O SLD matched to d-PSS, and the other was in D_2O/H_2O SLD matched to PEDOT. Given that DYMAP is a surfactant, and that the technical data sheet of DYMAP provided by the supplier states that the critical micelle concentration of DYMAP is 0.1-0.4 mM at 25ºC, it is reasonable to assume that DYMAP forms micelles in polar solvents such as the one used in this study. To confirm this, the scattering data was analysed by fitting it to a

spherical form factor [55, 56], one of the simplest models for micelles. The scattering intensity is then described by equation 2

$$I_{(q)} = \frac{scale}{V} \cdot \left[3V(\Delta\rho) \cdot \frac{sin(qr) - qrcos(qr)}{(qr)^3} \right]^2 + B \qquad (2)$$

where *scale* is a volume fraction, V is the volume of the scatterer, r is the radius of the sphere, $\Delta\rho$ is the difference between the SLDs of the scatterer and the solvent, and B is the background scattering. As shown by figure 3, the scattering profile of both solutions is very similar with the only clear difference being the intensity. As discussed before, this is due to the difference in contrast between DYMAP and each subtracted solvent. Since the SLD of DYMAP is 4.67×10^{-8} Å^{-2}, the solution with a D_2O/H_2O solvent matched to d-PSS (SLD is 4.18×10^{-6} Å^{-2}) has a higher contrast than the one in which DYMAP is dissolved in a D_2O/H_2O solvent matched to PEDOT (SLD 1.80×10^{-6} Å^{-2}). This results in a higher intensity scattering signal from DYMAP when it is in the d-PSS matched D_2O/H_2O solvent. More importantly, the sphere model fitted the data very well and resulted in a radius that was virtually the same for both samples. This was expected given that the scattering object, DYMAP, is the same in both solutions. As shown in table 2, the radius of the d-PSS matched sample was 25.7 ± 0.0379 Å and the radius of the PEDOT matched sample was 25.4 ± 0.3053 Å. The radii are in reasonable agreement with the theoretically estimated length of DYMAP (by adding up the standard values for every bond length in the backbone of DYMAP) which is ~28 Å. This is strong evidence that DYMAP forms micelles in aqueous solvents. Moreover, the molecular weight and the average micellar molecular weight of DYMAP are 363.6 and 30,200 respectively which means that, on average, there are ≈80 molecules of DYMAP per micelle.

While, according to the evidence presented above, DYMAP forms micelles in water, it is known that in the presence of additives with asymmetrically distributed charges such as salts, surfactant micelles in solutions can grow from spherical, elliptical, or cylindrical objects to long worm-like micelles [57]. This phenomena is driven by thermodynamics and the length and number of worm-like micelles are dependant on the concentration of the additive which, at very high concentrations, results in gelation. Due to the polyelectrolyte nature of

PEDOT:d-PSS, it is proposed that a similar effect occurs to DYMAP in the presence of PEDOT:d-PSS. Such an effect could then be responsible for the change in the interchain distance between charged d-PSS segments induced by the addition of DYMAP.

It is proposed that at low DYMAP doping concentrations from 5 mM to 15 mM, DYMAP starts to form short worm-like micelles in the presence of PEDOT:d-PSS. These worm-like micelles grow as more DYMAP is added, however, up to 15 mM they are significantly smaller than the interchain distance between the negatively charged d-PSS segments. Above 15 mM concentration, the DYMAP worm-like micelles grow long enough to start pushing the charged d-PSS chains apart due to steric hindrance. This effect is corroborated by the linear decrease of q_0 as a function of the dopant concentration above 15 mM which indicates that as the worm-like micelles grow longer with the addition of DYMAP, the charged d-PSS chains are proportionally pushed apart. At 30 mM doping concentration the DYMAP worm-like micelles have grown long enough to overcome steric hindrance and attach to the negatively charged d-PSS segments. This can be attributed to the quaternary ammonium cation in DYMAP which gets coulombically attached to the negatively charged d-PSS segments. This effect, in which an asymmetrically charged dopant is attached by its positive charge to the negatively charged backbone PSS segments of PEDOT:PSS, has been widely reported in literature [23-26, 28, 29, 29-31]. The coulombic interaction between the positive cation of DYMAP and the negatively charged d-PSS segment results in the relaxation of the backbone segments previously stressed by the steric hindrance caused by the growing DYMAP wormlike micelles. The existence and growth of DYMAP worm-like micelles are further supported by the observed gelation of the PEDOT:PSS dispersion at 30 mM doping concentration which indicates that at this concentration the DYMAP worm-like micelles have grown long enough to bridge separate strands of d-PSS resulting in the cross-linking of the d-PSS chains, and thus, the formation of a gel network. Figure 4 illustrates a schematic representation of the effects described above.

Now, the screening length (ξ) is analysed. In semi-dilute solutions whereby a chain has been labelled with deuteration, the correlation length can be defined as the size of a blob where the chain does not interact with other chains [58]. For polyelectrolytes this can be interpreted as the average size of screening diameter caused by neutralised objects, which for

PEDOT:d-PSS are the d-PSS neutralised chain segments that have the PEDOT oligomers attached along their length. The ξ of pristine d-PSS was 41.16 Å. Upon adding 5 mM DYMAP doping the screening length of the neutralised d-PSS chains stays virtually the same at 41.40 Å which indicates that this amount of DYMAP is insufficient to induce any alterations to the original ξ of neutralised d-PSS. At 10 mM and 15 mM doping concentration the ξ to increase by ~ 12 ξ relative to pristine d-PSS, and further addition of DYMAP at 20 mM and 25 mM concentration the ξ increases to increases to 62.90 Å and 64.81 Å respectively. Lastly, at the maximum doping concentration of 30 mM, the ξ increases considerably more to 110.07 Å, however the wide uncertainty (±63.09 Å) in this value makes it difficult to determine the magnitude of this increase. In order to explain the change in ξ as a function of DYMAP concentration, the focus is turned again to the formation of worm-like micelles by DYMAP due to its surfactant characteristic. As mentioned above, this is an effect driven by thermodynamics since forming worm-like micelles is probably the most energetically favourable action for the DYMAP micelles in the presence of the charged PEDOT:d-PSS. However, when the micelles are in very close proximity to the negatively charged d-PSS backbone segments, the quaternary ammonium cation in DYMAP can be attracted to the negatively charge in d-PSS, which results in the coulombic binding of DYMAP and the negatively charged d-PSS segments. Therefore, a possible explanation for the increased ξ as a function of the concentration then, is the slow gradual attachment of DYMAP micelles to the negatively attached d-PSS backbone as the concentration of DYMAP increases. While the formation of worm-like micelles is the primary and most energetically favourable action for DYMAP when introduced into the PEDOT:d-PSS dispersion, a lesser amount of DYMAP ends attaching to the negatively charged d-PSS backbone segments. This results in a low amount of DYMAP worm-like micelles growing from the d-PSS backbone some of which will grow long enough as more DYMAP is added to connect with other worm-like micelles formed either in other d-PSS backbones or in self-assembled worm-like micelles. More importantly, the slow attachment of DYMAP to the negatively charged d-PSS backbone segments results in the slight neutralisation of those segments which consequently results in the extension of the screening reach of d-PSS. We can see in figure 2, by the gradual increase in the correlation length, the slow and gradual attachment of a small amount of DYMAP particles as the concentration is increased. At 30 mM, however, this effect is

increased significantly since the DYMAP fibril network is formed and the crosslinking induced by DYMAP produces a significantly increased ξ from the d-PSS segments.

CONCLUSIONS

By deuterating the PSS moiety in PEDOT:PSS to make PEDOT:d-PSS and using SANS, we determined the effect that the zwitterionic dopant DYMAP has on the spacing between the d-PSS chains in a PEDOT:d-PSS dispersion. It was found that DYMAP forms micelles in water, and it was proposed that when in the presence of PEDOT:d-PSS, DYMAP grows into worm-like micelles as the concentration of DYMAP is increased up to the point of gelation of the dispersion. The interchain distance between negatively charged d-PSS backbone segments remains virtually unaffected by the DYMAP worm-like micelles up to 15 mM DYMAP concentration, however, as more dopant is added the worm-like micelles grow long enough to increase the interchain distance between negatively charged d-PSS segments due to steric hindrance. At 30 mM however, the DYMAP worm-like micelles grow long enough to form an interconnected network with the d-PSS chains by coulombically interacting with them which results in the relaxation of d-PSS chains and a decrease in the interchain distance between them. The screening length of the neutralised d-PSS segments that are attached to the PEDOT oligomers increases as DYMAP concentration is increased as a result of the slow and partial neutralisation of some negatively charged d-PSS. This effect is greatly improved at 30 mM when the gelation of the dispersion occurs due to the interconnected DYMAP network significantly screening the negatively d-PSS backbone segments. These findings provide insight on the structural modificaiton of PEDTOT:PSS by zwitterionic surfactant doping contributing to the progress in understanding the origin of conductivity enhancement of PEDOT:PSS.

REFERENCES

1.   L. Groenendaal, F. Jonas, D. Freitag, H. Pielartzik, J. R. Reynolds, Adv. Mater. **12**(7), 481 (2000). DOI: 10.1002/(SICI)1521-4095(200004)12:7<481::AID-ADMA481>3.0.CO;2-C

2.   J. Kawahara, P.A. Ersman, I. Engquist, M. Berggren, Org. Electron. **13**(3), 469 (2012). DOI: 10.1016/j.orgel.2011.12.007

3.   T.-H. Han, S.-H- Jeong, Y. Lee, H.-K Seo, S.-J Kwon, M.-H Park, T.-W- Lee, J. Inf. Disp. **16**(2), 71 (2015). DOI: 10.1080/15980316.2015.1016127

4.   R. Po, C. Carbonera, A. Bernardi, N. Camaioni, Energy Environ. Sci. **4**, 285 (2011). DOI: 10.1039/C0EE00273A

5.   C. K. Kwak, G. E. Pérez, B. G. Freestone, S. A. Al-Isaee, A. Iraqi, D. G. Lidzey, A. D. F. Dunbar, J. Mater. Chem. C, **4**(45), 10722 (2016). DOI: 10.1039/C6TC03771B

6.   S. Khan, M. Ul-Islam, M. W. Ullah, Y. Kim, J. K. Park, Cellulose. **22**(4), 2141 (2015). DOI: 10.1007/s10570-015-0683-2

7.   S.-C. Luo, E. Mohamed Ali, N. C. Tansil, H.-H. Yu, S. Gao, E. A. B. Kantchev, J. Y. Ying, Langmuir. **24**(15), 8071 (2008). DOI: 10.1021/la800333g

8.   S. M. Richardson-Burns, J. L. Hendricks, D. C. Martin, J. Neural. Eng. **4**(2), L6 (2007). DOI: 10.1088/1741-2560/4/2/L02

9.   J. Yang, D. H. Kim, J. L. Hendricks, M. Leach, R. Northey, D. C. Martin, Acta Biomater. **1**(1), 125 (2005). DOI: 10.1016/j.actbio.2004.09.006

10.   Y. Xiao, D. C. Martin, X. Cui, M. Shenai, Biotechnol. Appl. Biochem. **128**(2), 117 (2006). DOI: 10.1385/ABAB:128:2:117

11.   M. Hokazono, H. Anno, N. Toshima, J. Electron. Mater. **43**(6), 2196 (2014). 10.1007/s11664-014-3003-y

12.   C.-K Cho, W.-J. Hwang, K. Eun and S.-H. Choa, S.-I. Na, H.-K. Kim, Sol. Energy Mater Sol. Cells, **95**(12), 3269 (2011). DOI: 10.1016/j.solmat.2011.07.009

13.	E. Vitoratos, S. Sakkopoulos, E. Dalas, N. Paliatsas, D. Karageorgopoulos, F. Petraki, S. Kennou, S.A. Choulis, Org. Electron. **10**(1), 61 (2009). DOI: 10.1016/j.orgel.2008.10.008

14.	M. Dietrich, J. Heinze, G. Heywang, F. Jonas, J. Electroanal. Chem. **369**(1-2), 87 (1994). DOI: 10.1016/0022-0728(94)87085-3

15.	M. Dobbelin, R. Marcilla, M. Salsamendi, C. Pozo-Gonzalo, P. M. Carrasco, J. A. Pomposo, D. Mecerreyes, Chem. Mater. **19**(9), 2147 (2007). DOI: 10.1021/cm070398z

16.	C. Badre, L. Marquant, A. M. Alsayed, L. A. Hough, Adv. Funct. Mater. **22**(13), 2723 (2012). DOI: 10.1002/adfm.201200225

17.	Y. Xia, J. Ouyang, ACS Appl. Mater. Interfaces. **2**(2), 474 (2010). DOI: 10.1021/am900708x

18.	C.-C. Lin, C.-K. Huang, Y.-C. Hung, M.-Y- Chang, Jpn. J. Appl. Phys. **55**(8), 081602 (2016). DOI: 10.7567/JJAP.55.081602

19.	J. S. Yang, S. H. Oh, D. L. Kim, S. J. Kim, H. J. Kim, ACS Appl. Mater. Interfaces. **4**(10), 5394 (2012). DOI: 10.1021/am301320m

20.	Z. Hu, J. Zhang, Z. Hao, Y. Zhao, Sol. Energy Mater Sol. Cells. **95**(10), 2763 (2011). DOI: 10.1016/j.solmat.2011.04.040

21.	D. Alemu, H.-Y. Wei, K.-C. Ho, C.-W- Chu, Energy Environ. Sci. **5**(11), 9662 (2012). DOI: 10.1039/C2EE22595F

22.	C. Girotto, D. Moia, B. P. Rand, P. Heremans, Adv. Funct. Mater. **21**(1), 64 (2011). DOI: 10.1002/adfm.201001562

23.	Z. Zhao, Q. Wu, F. Xia, X. Chen, Y. Liu, W. Zhang, J. Zhu, S. Dai, S. Yang, ACS Appl. Mater. Interfaces. **7**(3), 1439 (2015). DOI: 10.1021/am505387q

24.	Y. Xia, J. Ouyang, Org. Electron. **11**(6), 1129 (2010). DOI: 10.1016/j.orgel.2010.04.007

25.	Y. Xia, J. Ouyang, Macromolecules. **42**(12), 4141 (2009). DOI: 10.1021/ma900327d

26.	Z. Fan, D. Du, Z. Yu, P. Li, Y. Xia, J. Ouyang, ACS Appl. Mater. Interfaces. **8**(35), 23204 (2016). DOI: 10.1021/acsami.6b07234

27.	G. Fang, S. Wu, Z. Xie, Y. Geng, L. Wang, Macromol. Chem. Phys. **212**(17), 1846 (2011). DOI: 10.1002/macp.201100102

28.	Y. Xia, H. Zhang, J. Ouyang, J. Mater. Chem. **20**(43), 9740 (2010). DOI: 10.1039/C0JM01593H

29. Z. Zhao, X. Chen, Q. Liu, Q. Wu, J. Zhu, S. Dai, S. Yang, Org. Electron. **27**, 232 (2015). DOI: 10.1016/j.orgel.2015.09.022

30. J. Ouyang, Displays. **34**(5), 423 (2013). DOI: 10.1016/j.displa.2013.08.007

31. J. Y. Kim, J. H. Jung, D. E. Lee, J. Joo, Synth. Met. **126**(2-3), 311 (2002). DOI: 10.1016/S0379-6779(01)00576-8

32. Y. Xia, J. Ouyang, J. Mater. Chem. **21**(13), 4927 (2011). DOI: 10.1039/C0JM04177G

33. X. Crispin, F. L. E. Jakobsson, A. Crispin, P.C.M. Grim, P. Andersson, A. Volodin, C. Van Haesendonck, M. Van Der Auweraer, W.R. Salaneck, M. Berggren, Chem. Mater. **18**(18), 4354 (2006). DOI: 10.1021/cm061032+

34. M. N. Gueye, A. Carella, N. Massonnet, E. Yvenou, S. Brenet, J. Faure-Vincent, S. Pouget, F. Rieutord, H. Okuno, A. Benayad, R. Demadrille, J.-P- Simonato, Chem. Mater. **28**(10), 3462 (2016). DOI: 10.1021/acs.chemmater.6b01035

35. T. Etampawala, M. Tehrani, A. Nematollahi, L. He, M. Dadmun, Org. Electron. **51**, 86 (2017). DOI: 10.1016/j.orgel.2017.08.030

36. D. Bagchi, R. Menon, Chem. Phys. Lett. **425**(1-3), 114 (2006). DOI: 10.1016/j.cplett.2006.05.014

37. T. Takano, H. Masunaga, A. Fujiwara, H. Okuzaki, T. Sasaki, Macromolecules. **4**(45), 10722 (2016). DOI: 10.1039/C6TC03771B

38. Z. Zhao, W. Zhang, X. Zhao, S. Yang, Organic Solar Cells materials, devices, interfaces, and modeling, Boca Raton: CRC Press, 2015, London.

39. R. J. Murphy, K. M. Weigandt, D. Uhrig, A. Alsayed, C. Badre, L. Hough, M. Muthukumar, Macromolecules. **48**(24), 8989 (2015). DOI: 10.1021/acs.macromol.5b02320

40. S.T. Lee, Z.Q. Gao, L.S. Hung, Appl. Phys. Lett., **75**(10), 1404 (1999). DOI: 10.1063/1.124708

41. G. E. Pérez, G. Bernardo, H. Gaspar, J. F. K. Cooper, F. Bastianini, A. J. Parnell, A. D. F. Dunbar, ACS Appl. Mater. Interfaces. **11**(4), 13803 (2019). DOI: 10.1021/acsami.9b02700

42. M. Lefebvre, Z. Qi, D. Rana, P. G. Pickup, Chem. Mater. **11**(2), 262 (1999). DOI: 10.1021/cm9804618

43. F. Jonas, G. Heywang, Electrochim. Acta. **39**(8-9), 1345 (1994). DOI: 10.1016/0013-4686(94)E0057-7

44.   LOQ   Specifications,
https://www.isis.stfc.ac.uk/Pages/Loq-technical-information.aspx, Last accessed: 07-05-2019

45.   O. Arnold et al., Nucl. Instrum. Methods Phys. Res. A. **764**, 156 (2014). DOI:
10.1016/j.nima.2014.07.029

46.   Broad Peak Model, http://www.sasview.org/docs/user/models/broad_peak.html, Last
accessed: 07-05-2019

47.   SasView Software, http://www.sasview.org/, Last accessed: 07-05-2019

48.   NIST Centre for Neutron Research Neutron activation and scattering calculator,
https://www.ncnr.nist.gov/resources/activation/, Last accessed: 05-05-2019

49.   F. Horkay, B. Hammouda, Colloid Polym. Sci. **286**(6-7), 611 (2008). DOI:
10.1007/s00396-008-1849-3

50.   N. Ise, T. Okubo, Acc. Chem. Res. **13**(9), 303(1980). DOI: 10.1021/ar50153a002

51.   M. Nierlich, C. E. Williams, F. Boue, J. P. Cotton, M. Daoud, B. Famoux, G. Jannink,
C. L. Picot, M. Moan, C. Wolff, M. Rinaudo, P. G. de Gennes, J. Phys. **40**(7), 701 (1979).
DOI: 10.1051/jphys:01979004007070100

52.   M. Nierlich, F. Boue, A. Lapp, R. Oberthür, Colloid Polym. Sci. **263**(12), 955 (1985).
DOI: 10.1007/BF01410988

53.   M. Drifford, J. P. Dalbiez, J. Phys. Chem. **88**(22), 5368 (1984). DOI:
10.1021/j150666a052

54.   P.-G. de Gennes, P. Pincus, R. M. Velasco, F. Brochard, F, J. Phys. **37**(12), 1461
(1976). DOI: 10.1051/jphys:0197600370120146100

55.   Sphere model, http://www.sasview.org/docs/user/models/sphere.html, Last accessed:
30-05-2019

56.   A. Guiner, G. Fournet, C. Walker, K. L. Yudowitch, Jahn Willey-Champan, Small
Angle Scattering of X-Rays, 1955, New-York

57.   S. R. Raghavan, Langmuir. **25**(15), 8382 (2009). DOI: 10.1021/la901513w

58.   P.-G. De Gennes, P.-G- Gennes, Scaling Concepts in Polymer Physics, Cornell
university press, 1979

Figure captions.

Fig. 1. 1D SANS plots and corresponding fits (broad peak model) of pristine and different concentration DYMAP doped PEDOT:d-PSS. Samples were synthesised (and hence dispersed) in a solvent which SLD matches that of PEDOT to obtain information on d-PSS.

Fig. 2. Screening length, peak position, and interchain distance as a function of DYMAP doping concentration on PEDOT:d-PSS resulting from the Broad Peak model fits. Samples were synthesised (and hence dispersed) in a solvent which SLD matches that of PEDOT to obtain information on d-PSS.

Fig. 3. 1D SANS plots and corresponding fits (Sphere model) of 30 mM DYMAP aqueous solutions.

Fig. 4. Schematic representation of the behaviour of DYMAP and its effects on the PEDOT:d-PSS dispersion. The colour of the solutions is shown only for demonstration purposes, and do not represent the actual change of colour of the solutions.
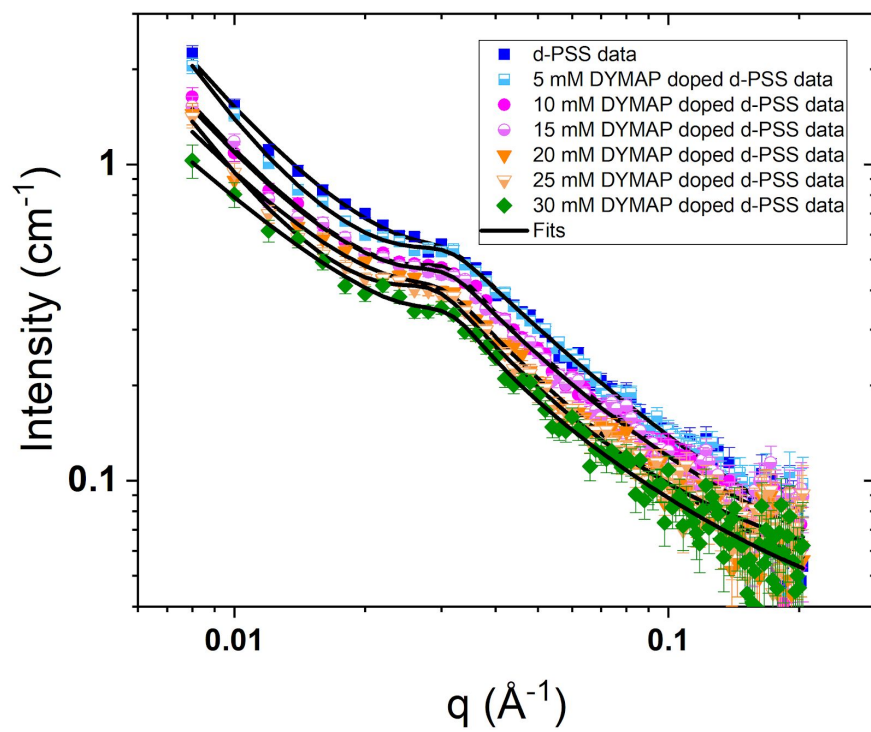
Fig. 1. G. E. Pérez, *Journal of Surface Investigation: X-ray, Synchrotron and Neutron Techniques*
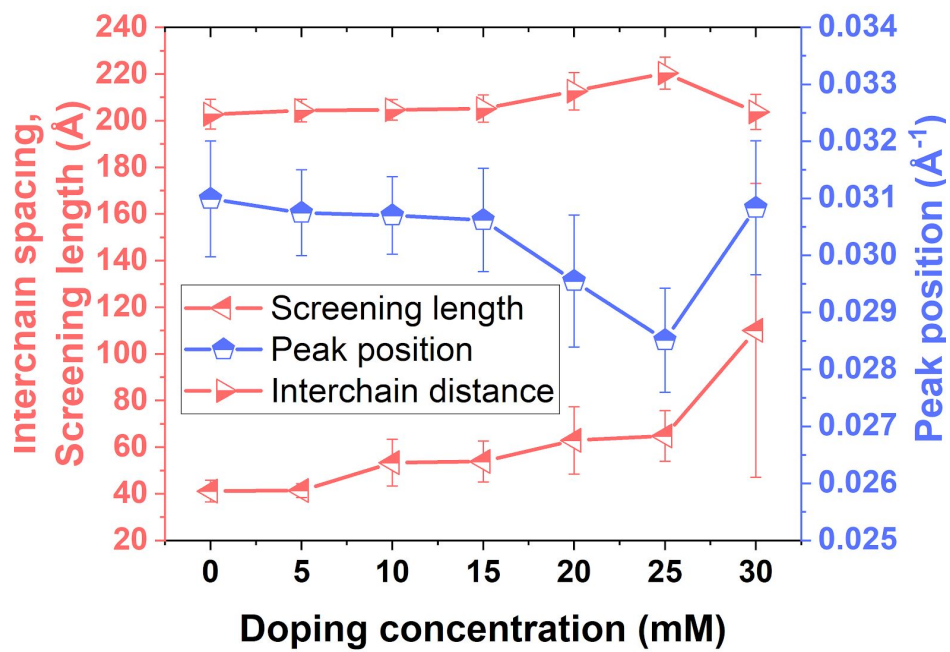
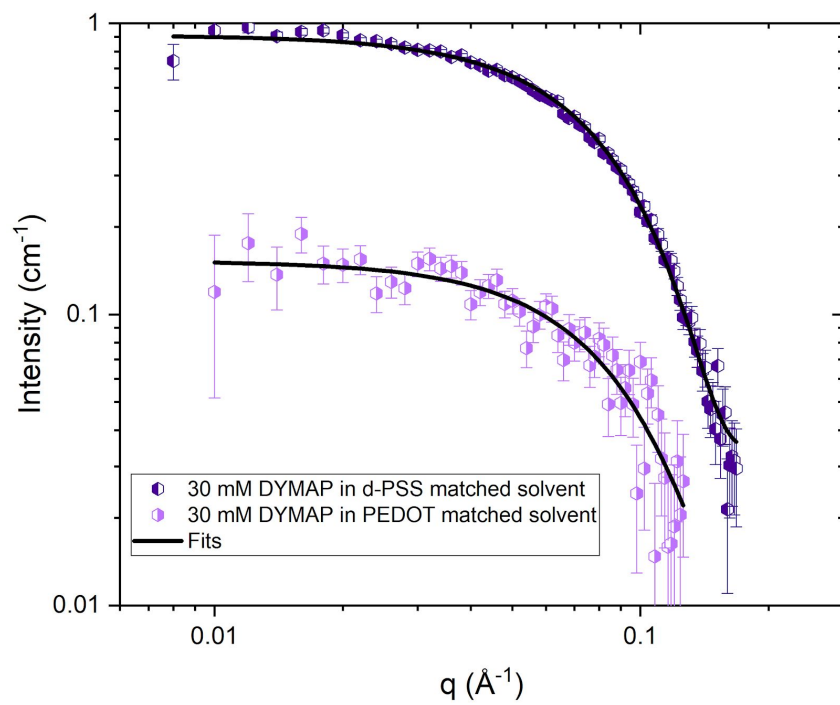Fig. 2. G. E. Pérez, Journal of Surface Investigation: X-ray, Synchrotron and Neutron Techniques

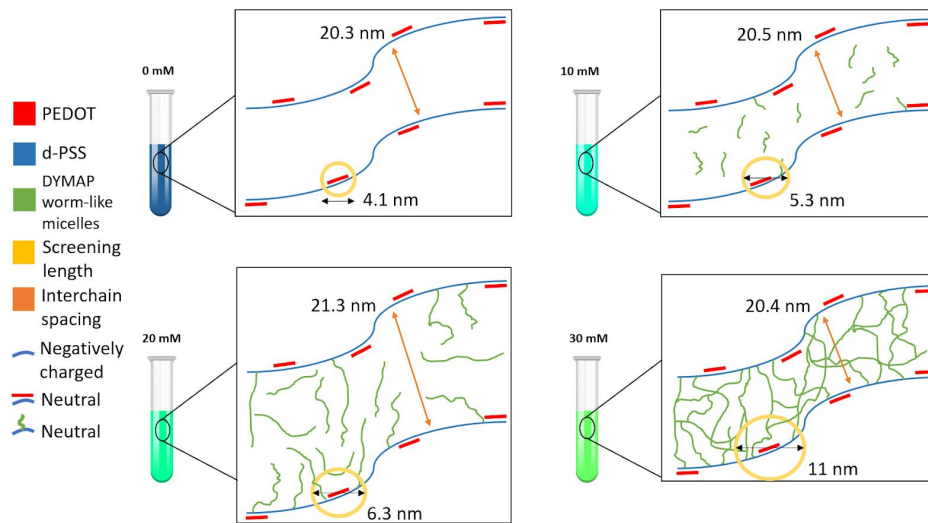Fig. 3. G. E. Pérez, Journal of Surface Investigation: X-ray, Synchrotron and Neutron Techniques

Fig. 4. G. E. Pérez, Journal of Surface Investigation: X-ray, Synchrotron and Neutron Techniques

Table 1. Parameters resulting from the Broad Peak model fits of pristine and different concentration DYMAP doped PEDOT:d-PSS. Samples were synthesised (and hence dispersed) in a solvent which SLD matches that of PEDOT to obtain information on d-PSS.

Doping Concentration (mM)	ξ, Screening length (Å)	q_0, peak position (Å^{-1})	A, Porod law scale factor	n, Low-q scaling factor	C, Lorentzian scale factor	m, High-q scaling factor	χ^2, quality of the fit
Pristine	41.16±4.62	3.10±0.10 (x 10^{-2})	8.56±4.98 (x 10^{-4})	1.58±0.12	-0.35±0.04	-1.01±0.16	0.7603
5	41.40±2.98	3.08±0.08 (x 10^{-2})	1.99±1.13 (x 10^{-4})	1.86±0.12	-0.41±0.03	-1.05±0.12	0.7308
10	53.35±10.04	3.07±0.07 (x 10^{-2})	6.30±4.26 (x 10^{-4})	1.57±40.14	-0.37±0.05	-0.80±0.16	0.6080
15	53.84±8.77	3.06±0.09 (x 10^{-2})	7.18±5.32 (x 10^{-4})	1.53±0.16	-0.30±0.03	-1.04±0.16	0.9555
20	62.90±14.44	2.96±0.12 (x 10^{-2})	1.26±1.19 (x 10^{-3})	1.39±0.20	-0.22±0.05	-1.16±0.18	0.9005
25	64.81±10.88	2.85±0.09 (x 10^{-2})	1.73±1.61 (x 10^{-4})	1.80±0.20	-0.28±0.03	-1.11±0.17	0.7589
30	110.13±63.03	3.08±0.12 (x 10^{-2})	3.12±3.26 (x 10^{-3})	1.17±0.22	0.15±0.06	1.10±0.42	0.6465

Table 2. Parameters resulting from fitting the Sphere model to the 1D scattering plots of 30 mM DYMAP aqueous solutions. The SLDs of DYMAP and the solvent were fixed to the theoretical values calculated using the NIST center for Neutron Research online database. All the other parameters were fitted.

	DYMAP in solvent matched to d-PSS	DYMAP in solvent matched to PEDOT
Scale	$7.20\pm0.10(\text{x } 10^{-3})$	$6.71\pm2.06(\text{x } 10^{-3})$
Background (cm^{-1})	$3.54\pm0.12(\text{x } 10^{-2})$	$1.03\pm0.21(\text{x } 10^{-2})$
SLD DYMAP ($1 \text{ x } 10^{-6}$ Å^{-2})*	0.0467	0.0467
SLD Solvent ($1 \text{ x } 10^{-6} \text{ Å}^{-2}$)*	4.18	1.80
Radius (Å)	25.68 ± 0.0379	25.43 ± 0.3053

*Calculated using the NIST Center for Neutron Research online database [48]